



# Exploring the Relationship Between Land Use Land Cover and Land Surface Temperature: a Case Study in Bangladesh and the Policy Implications for the Global South

Annyca Tabassum<sup>1</sup> · Rony Basak<sup>1</sup> · Wanyun Shao<sup>2,3</sup> · Md Munjurul Haque<sup>2,3</sup> · Tahmid Anam Chowdhury<sup>1</sup> · Hemal Dey<sup>2,3</sup>

Accepted: 14 August 2023  
© The Author(s), under exclusive licence to Springer Nature Switzerland AG 2023

## Abstract

Changes in land use and land cover (LULC) have a considerable impact on land surface temperature (LST) and they are a major driver of climate change. Comprehending the relationship between LULC and LST is crucial when developing effective measures to mitigate the effects of climate change, especially since people in the global south are particularly vulnerable. This study aimed to assess the relationship between LULC and LST in the Barapukuria coal mining region of Bangladesh using Landsat satellite images from 1990 to 2020. Specifically, the study evaluated the distribution of LST in various landforms, developed a cross-sectional profile, and investigated the impact of LULC on LST. The study's findings indicate a significant conversion of vegetated areas into urban spaces. Over the past 30 years, approximately 56% of the agricultural land in the study area has been converted into settlements and bare land. The area of bare land and settlements expanded by 16% and 11%, respectively, while the areas of agricultural land and vegetation dropped by 24% and 4%, respectively. LST was found to increase with the expansion of bare land and human settlements, with the maximum mean temperature observed for bare land in 2020 at 23.02 °C. Zonal statistics and correlation analysis established a significant positive correlation between LST and settlements, as well as bare land. The results suggest that changes in LULC significantly influence variations in LST, leading to temperature increases as bare land and settlements expand. Additionally, we found that agricultural land had a lower LST compared to other land cover types, possibly due to evapotranspiration. Our research suggests that to create effective policies for climate change mitigation and adaptation, policymakers in the global south need to use a holistic approach that considers the relationships between LULC and LST. We also recommend that policy interventions focus on promoting urban green spaces, encouraging sustainable agriculture practices, and regulating urban expansion and deforestation to mitigate the adverse effects of climate change.

**Keywords** LULC · LST · Coal mine · Urbanization · Climate change mitigation · Sustainable development

## Introduction

Changes in LULC are occurring at an unprecedented rate around the world, particularly in the developing nations in the global south, like Bangladesh (Morshed et al. 2023).

✉ Md Munjurul Haque  
mdmunjurulhaque@gmail.com

<sup>1</sup> Department of Geography and Environment, Shahjalal University of Science and Technology, Sylhet 3114, Bangladesh

<sup>2</sup> Department of Geography, The University of Alabama, Tuscaloosa, AL, USA

<sup>3</sup> Alabama Water Institute, Tuscaloosa, AL, USA

There are significant environmental, economic, and social effects associated with the conversion of natural land cover types into agricultural lands, urban areas, and other land uses (Bajocco et al. 2012). Changes in LULC have broader effects on climate change on a global scale in addition to having an impact on local ecosystems and human well-being (Roy et al. 2022). These effects will be particularly pronounced in densely populated developing nations of the global south, such as Bangladesh (Hussain et al. 2016). One of the most significant effects of LULC modifications, which contributes to global climate change, is the resulting shift in LST (Ranganage et al. 2019). The Earth's radiation budget represents the equilibrium between incoming solar radiation and outgoing thermal radiation. It can be impacted by the reduction of LULC such as vegetation or forest due to rapid urbanization,

leading to a rise in temperature and global warming (Hu et al. 2016). Furthermore, activities such as burning fossil fuels, removing vegetation, and other practices associated with coal mining worsen the impact on LULC changes, thereby contributing to climate change (Derome and Lukina 2010). LULC and LST studies have evolved into more crucial tools in the present to address those pressing concerns and the adverse effects of climate change through global monitoring and measurement (Roxburgh et al. 2020; Balogun and Ishola 2017; Ahmed 2011; Lilly Rose and Devadas 2009; Ahmed et al. 2022; Chowdhury and Islam 2022). Modern techniques like remote sensing (RS) and geographical information systems (GIS) are crucial for identifying LULC and LST (Choudhury et al. 2019). Satellite images have been employed to quantify vegetation loss, monitor crop adversities, and investigate various environmental events. They provide faster, more cost-effective, and more precise data compared to conventional approaches (Skole and Tucker 1993; Kachhwala 1985). Combining RS and GIS technologies enables efficient analysis, monitoring, and simulation of LULC and LST fluctuations (Fu and Weng 2018; Niyogi 2019; Thapa and Murayama 2009; Trolle et al. 2019), thereby contributing to a comprehensive understanding of LULC changes and LST variations (Hathout 2002).

On a global scale, anomalies in LST have been detected due to LULC variations in mining regions (Cao et al. 2020; Chaddad et al. 2022; Rajasekar and Weng 2009). However, there are no LST-LULC-based studies that have been undertaken in the mining region of Bangladesh, although there have been a few studies on LST changes owing to deforestation in the Rohingya-influxes region of Bangladesh (Hasan et al. 2023; Bappa et al. 2022; Mahi et al. 2021; Rashid et al. 2021). Due to mining activities and the thermal power plant project, the land use pattern in the research region has evolved, resulting in the deterioration of natural ecosystems and irreversible changes to the environment (Saini et al. 2016). The geography, habitat, and biological community of the research region have changed significantly due to the mining industry and power plants (Hossain et al. 2015). LST plays a critical role in determining the microclimate, and its excessive heat can have devastating effects on humans and the environment, such as elevated health risks and increased energy consumption (Adiguzel et al. 2022; Cetin et al. 2018). Despite the importance of studying the environmental impacts of coal mines and coal-fired power plants, a limited number of studies have been done to analyze the relationship between landform change and development activities (Adiguzel et al. 2022; Cetin et al. 2018). Consequently, it is essential to investigate the qualitative and quantitative effects of urbanization on climate change in the research area, as well as their future consequences. This study attempts to detect the temporal variations in LST across distinct

land cover areas (LCAs) in the thermal power plant area. In addition, the research will investigate the relationship between LST and LULC and shed light on how the private sector's large-scale mining operations and power production industry have dramatically altered the LULC of the once densely vegetated, biologically diverse, and confined coal reserve area.

The aim of this study will focus on the following objectives: (i) To study LULC change in the Barapukuria coal mine area from 1990 to 2020, (ii) to study LST change from 1990 to 2020, and (iii) to investigate the relationship between LULC and LST. The study's conclusions will have significant policy ramifications for Bangladesh and other developing nations in the global south dealing with comparable LULC issues. To reduce the adverse effects of LULC changes and promote sustainable development, the conclusions drawn from this study will be valuable information for policymakers and planners in making decisions about land use planning, natural resource management, and urban development.

## Methodology

### Description of the Study Area

The study area includes the Barapukuria coal mine, the coal-fired thermal power station, a water reservoir, and a forest region. These were identified using the buffering approach. The Barapukuria coal mine and coal-fired thermal power station are situated in the Hamidpur Union, Parbotipur Upazila, in the northwestern part of Bangladesh. They are located about 50 km southeast of the Dinajpur district and 20 km east of the border with India. The area under investigation is delineated by the coordinates  $25^{\circ}31'45''$  to  $25^{\circ}35'05''$ N and  $88^{\circ}55'48''$  to  $88^{\circ}59'53''$ E. These coordinates are depicted on Bangladesh's topographic sheet number 78C/14 (scale 1:50,000) (Fig. 1). This area is in the Northwestern climatic zone of Bangladesh. According to the Köppen climate classification, this area experiences a tropical wet and dry climate. It undergoes a distinct monsoonal season, with an average annual temperature of  $25^{\circ}\text{C}$  ( $77^{\circ}\text{F}$ ), and monthly averages ranging from  $18^{\circ}\text{C}$  in January to  $29^{\circ}\text{C}$  in August. This area receives a total annual rainfall of 2001–2500 millimeters (mm) (Barry and Chorley 2009; Koppen 1936).

### Data Collection

Landsat satellite images from various years (1990, 2000, 2010, and 2020) were collected and compiled into a zip file sourced from the USGS website, aligning with the research

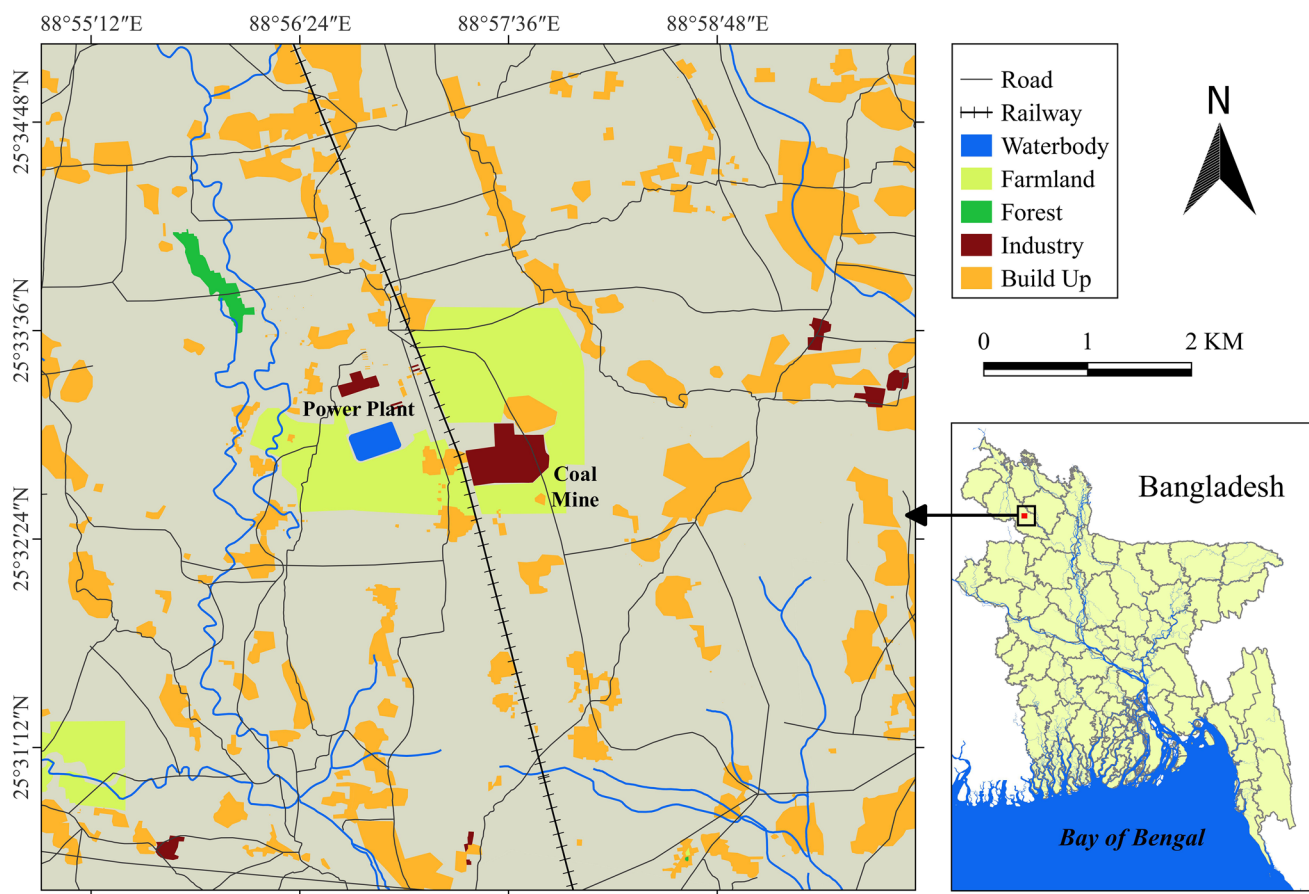


**Fig. 1** The location of the study area

objectives. Table 1 shows the details of the Landsat data used in this study. The Landsat TM or OLI/TIRS imagery was obtained using the Universal Transverse Mercator (UTM) projection within the 46N Datum World Geodetic System (WGS) 1984. All bands of Landsat images have a spatial resolution of 30 m.

## Data Processing

The entire analysis involved creating maps and visually analyzing the relationship between LULC and LST. Each dataset spanning from 1990 to 2020 underwent examination, and a concise generalization was derived to facilitate planning. The study's outcomes were analyzed after reviewing

each satellite's data. Subsequently, a comprehensive change detection analysis was conducted. Eventually, multiple approaches were employed to assess LST changes in the study area.

### LULC Change Detection Using Supervised Classification

Several methods of supervised classification exist, such as maximum likelihood, support vector machine, random forest, and artificial neural networks. For this study, we conducted maximum likelihood supervised classification using Erdas Imagine 2014 software. It is the most widely used method for analyzing multispectral satellite image data (Amare et al. 2023; Chughtai et al. 2021). This

**Table 1** Description of Landsat TM and OLI/TIRS images

Date and scan time	Satellite ID	Sensor ID	Path/row	Resolution	Cloud (%)
Jan 30, 1990	Landsat_5	TM	138/42	30	16
Jan 26, 2000	Landsat_5	TM	138/42	30	0
Feb 6, 2010	Landsat_5	TM	138/42	30	0
Feb 2, 2020	Landsat_8	OLI	138/42	30	0.39

method combines personal experience, interpretation of aerial imagery, map analysis, and fieldwork to identify and locate pre-existing LULC types (Jensen 1996). By utilizing the means and variances from training data, it calculates the probability of a pixel belonging to a certain class. Later, a certain pixel is assigned to the specific LULC category considering the maximum probability (Ozesmi and Bauer 2002).

This study aims to analyze the LULC categories in the study area to gain a better understanding of the spatial distribution and changes in land use patterns. The study area includes five LULC categories: agriculture land, vegetation, waterbody, settlement/built-up area, and bare land. Agriculture land consists of areas used for farming and crop cultivation, while vegetation encompasses areas of scattered plantations, including homestead areas. Waterbody includes areas covered by water, such as rivers, wetlands, and ponds. Settlement/built-up area comprises areas occupied by human settlements, while bare land consists of areas not covered by vegetation or water, including construction sites, development areas, and unoccupied land. By analyzing these categories, this study can provide valuable insights into the current state and potential future changes in land use patterns in the study area. After retrieving the data, the final step was image classification. As previously noted, the maximum likelihood parametric rule was utilized during classification.

A (Bayesian) probability function was derived from the inputs for classes generated from training sites based on statistics (mean; variance/covariance). Then, each pixel was assigned to the class to which it most likely matched. Following the classification process, the classified images underwent change detection analysis. Several change detection techniques are available in the literature including image differentiating (Koko et al. 2021), change vector analysis (Wang et al. 2020), and transition matrix (Bagwan and Sopan Gavali 2023). Since LULC data is categorical, the transition matrix method has become a widely employed technique for LULC detection. It visualizes pixel interchanges and calculates the area of transition. It is done using ENVI 5.3 software, where LULC raster datasets of two separate years have been used. The LULC transition matrix was generated using the Thematic Change Workflow function and pixel-by-pixel change statistics were produced.

**Accuracy Assessment** Accuracy assessment is a process of evaluating the accuracy or quality of the results obtained from a remote sensing or GIS analysis. It involves comparing the results obtained from the analysis with reference data, such as ground-truth data or previously existing data, to determine the level of accuracy and reliability of the analysis. Accuracy assessments based on thematic information

are used to determine the correctness of the supervised classification. To assess the accuracy of each area, a total of 250 random points were selected. This evaluation compares pixels or polygons generated from a classification map based on remotely sensed data and ground reference test data. Ground reference test data includes old toposheets and Google Earth historical images for the years 1990, 2000, and 2010. For the year 2020, intensive fieldwork was done in the study area from 17 November to 30 November 2020 to collect ground reference test data. Table 2 shows the overall accuracies of the identified images and kappa coefficients ( $K$ ) for the study area (1990, 2000, 2010, and 2020). The kappa coefficient reveals how a well-classified map and the reference data that goes with it agree.  $K$  values higher than 0.80 indicate high levels of accuracy; values between 0.40 and 0.80 indicate medium accuracy, while values below 0.40 indicate low levels of accuracy (Cui et al. 2022; Liu et al. 2020). The classification accuracy assessment demonstrates that it has changed over time. In this case, all the years have a kappa value greater than 0.80, indicating strong agreement. The spatial resolution associated with the LULC distribution significantly impacts classification accuracy. In summary, all the estimated results point to a positive outcome.

### LST Calculation

Surface radiant temperature is retrieved from thermal bands of TM and TIRS sensors (bands 6, 10, and 11). Bands 6, 10, and 11 have spectral ranges of 11.45  $\mu\text{m}$ , 10.8  $\mu\text{m}$ , and 12  $\mu\text{m}$  radiate from the earth's surface. As the images are level-one terrain-corrected (L1T) products, no additional rectification or correction is regarded in pre-processing (Ahmed 2011; Bonafoni et al. 2016). The LST was calculated from each thermal image and was compared between different periods.

$$L = \frac{L_{\max} - L_{\min}}{Q_{\text{cal}} - Q_{\min}} \times (Q_{\text{cal}} - Q_{\min}) + L_{\min} \quad (1)$$

where

$L$  = Sensor's aperture spectral radiance (in watts)

$L_{\max}$  = Scaled QCALMIN spectral radiance (in watts)

$L_{\min}$  = Scaled QCALMAX spectral radiance (in watts)

**Table 2** Overall accuracies (%) and kappa coefficients summary

Year	Overall accuracy	Kappa
1990	90.5	0.86
2000	94.7	0.90
2010	91.3	0.95
2020	93.1	0.96

$Q_{\text{cal}}$  = The quantized calibrated pixel value in digital numbers (DN)

$Q_{\text{min}}$  = The minimum quantized calibrated pixel value in digital numbers (DN)

**Calculation of LST from the Landsat 5** In the first step, the thermal band of Landsat 5 (band 6) was converted to radiation luminance (L) from the DN, which is mentioned in Equation (2). In the second step, at-satellite brightness temperature in Celsius was calculated from the radiation luminance (Landsat 2011), T (°C), using the following Equation (4):

$$T(C) = \frac{k_2}{\ln\left(\frac{k_1}{L} + 1\right)} - 273.15 \quad (2)$$

where  $k_1$  and  $k_2$  values of Landsat 5 are given in Table 3.

**Calculation of LST from the Landsat 8** The standard procedure to calculate LST from TIRS thermal band is to convert DN values (Landsat 2011) of the thermal bands (Band 10 in Landsat OLI/TIRS) into absolute radiance values.

$$L_\lambda = ML \times Q_{\text{cal}} + A_L \quad (3)$$

where

$L_\lambda$  = Spectral radiance ( $\text{W}/(\text{m}^2 * \text{sr} * \mu\text{m})$ )

$ML$  = Radiance multiplicative scaling factor for the band

$A_L$  = Radiance additive scaling factor for the band

$Q_{\text{cal}}$  = Level 1 pixel value in DN

In the second step, conversion from radiation luminance to at-satellite brightness temperature in Celsius, T (°C), was done, using the following Equation (4):

$$T_B(C) = \frac{k_2}{\ln\left(\frac{k_1}{L} + 1\right)} - 273.15 \quad (4)$$

where  $k_1$  and  $k_2$  values of Landsat 8 are given in Table 4.

The emissivity corrected LST was calculated after converting the brightness temperature values into degrees Celsius (°C) (Artis and Carnahan 1982; Weng et al. 2004), following Equation (5):

**Table 3** Calibration constants for TM and TIRS thermal bands

	$K_1 (\text{Wm}^{-2} \text{sr}^{-1} \mu\text{m}^{-1})$	$K_2 (k)$
TM	607.76	1260.56
OLI/TIRS	774.88	1321.08

**Table 4** Classification of the LST

Temperature class	Class range
Very low temperature	$LST \leq LST_{\text{mean}} - 1.5 \text{ STD}$
Low temperature	$LST_{\text{mean}} - 1.5 \text{ STD} < LST \leq LST_{\text{mean}} - \text{STD}$
Medium temperature	$LST_{\text{mean}} - \text{STD} < LST \leq LST_{\text{mean}} + \text{STD}$
High temperature	$LST_{\text{mean}} + \text{STD} < LST \leq LST_{\text{max}}$

$$LST(\text{°C}) = \frac{T_B}{1 + \left(\lambda \times \frac{T_B}{\rho}\right) \ln \varepsilon} \quad (5)$$

where

$T_B$  = Brightness temperature of Landsat 8 Band 10.

$\lambda$  = Emitted radiance wavelength ( $\lambda = 10.8 \mu\text{m}$ );  $\rho = h \times c/\sigma$  ( $1.438 \times 10 - 2 \text{ m K}$ ),  $\sigma$  = Boltzmann constant ( $1.38 \times 10 - 23 \text{ J/K}$ ),  $h$  = Planck's constant ( $6.626 \times 10 - 34 \text{ Js}$ ), and  $c$  = velocity of light ( $2.998 \times 108 \text{ m/s}$ ); and  $\varepsilon$  is the land surface emissivity, estimated using Equation (6) (Sobrino et al. 2004).

$$\varepsilon = mP_V + n \quad (6)$$

where  $m = (\varepsilon_v - \varepsilon_s) - (1 - \varepsilon_s) F\varepsilon_v$  and  $n = \varepsilon_s + (1 - \varepsilon_s) F\varepsilon_v$ , where  $\varepsilon_s$  and  $\varepsilon_v$  are the soil and vegetation emissivity, respectively. In this study, the results of Sobrino et al. (2004) for  $m$  (0.004) and  $n$  (0.986) were applied in the calculation.  $P_V$  is the vegetation proportion and was derived using Equation (8) (Carlson and Ripley 1997).

$$NDVI = \frac{NIR - Red}{NIR + Red} \quad (7)$$

$$P_V = \left( \frac{NDVI - NDVI_{\text{min}}}{NDVI_{\text{max}} - NDVI_{\text{min}}} \right)^2 \quad (8)$$

where  $NDVI$  is known as the normalized difference vegetation index calculated from the surface reflectance of near-infrared (NIR) and red bands.

**LST Zoning by Temperature Distribution** LST has been classified into multiple zones to identify low- to high-LST areas. Panah et al. (2017) suggested a scheme for LST zone classification (Table 4). Zoning is done from the maximum, mean, and standard deviation of LST of each year.  $LST_{\text{mean}}$  is the mean LST,  $LST_{\text{max}}$  is the maximum LST, and  $\text{STD}$  is the standard deviation of the specific year.

After the classification of each image's LST data, each class's LST value was calculated and the increasing or decreasing trend of each temperature class in the studied period was investigated. Moreover, LULC distribution for each zone was calculated for each year.

## LST and LULC Relation Assessment

To understand the relationship between LST and LULC, two approaches have been applied. First, zonal statistics have been done between LST and LULC using ArcMap 10.3. It includes a statistical summary of LST over each LULC class. Secondly, Pearson's correlation has been done between LST and biophysical parameters using R 4.1.3. Biophysical parameters include various indices that represent different land cover characteristics. In this study, it includes normalized difference vegetation index (NDVI), normalized difference built-up index (NDBI), dry bare soil index (DBSI), and normalized difference moisture index (NDMI) (Table 5). NDVI is widely used to assess the type and health of vegetation cover. NDBI is an index recognized to study built-up areas or concrete surfaces. The extent of dry bare soil or land is assessed by DBSI. Moisture is associated with water, and it may be available over any kind of LULC. Moisture over land cover is assessed by NDMI.

Mentioned indices include red, green, NIR, and short-wave infrared (SWIR) bands. NIR has 0.76–0.90  $\mu\text{m}$  wavelength. Red band has 0.63–0.69  $\mu\text{m}$  wavelength. SWIR1 has 1.55–1.75  $\mu\text{m}$  wavelength. Green band has 0.52–0.60  $\mu\text{m}$  wavelength.

**Table 5** Biophysical parameters to relate with LST

Index	Equation	Reference
NDVI	$\frac{(NIR-Red)}{(NIR+Red)}$	Rouse Jr et al. 1974
NDBI	$\frac{(SWIR1-NIR)}{(SWIR1+NIR)}$	Zha et al. 2003
DBSI	$\frac{(SWIR-Green)}{(SWIR+Green)} - NDVI$	Rasul et al. 2018
NDMI	$\frac{(NIR-SWIR)}{(NIR+SWIR)}$	Wilson and Sader 2002

## Results and Discussion

### LULC Change Analysis

Table 6 displays the overall temporal change for different LULC categories between 1990 and 2020. This table provides detailed information about the change in area (in hectares) and percentage of change for three temporal scale: 1990–2000, 2000–2010, and 2010–2020.

The temporal analysis of LULC changes reveals that in the last three decades, the pattern of LULC has changed significantly in Barapukuria. Such as, agricultural land has experienced a significant loss in the last 30 years (1990–2020) with net loss of 23.94% (1434.42 ha). Furthermore, bare land has dramatically increased 15.94% (1042.83 ha), vegetation experienced a slight decrease by 3.52% (208.71 ha), settlement increased by 11.05% (721.08 ha), and water bodies faced a small increase by 0.49% (34.56 ha) overall.

Figure 2 depicts the spatio-temporal changes of LULC in the study area over the last 30 years. From 1990 to 2020, agricultural land, vegetation, and water bodies have decreased, and in contrary, bare land and settlement have increased.

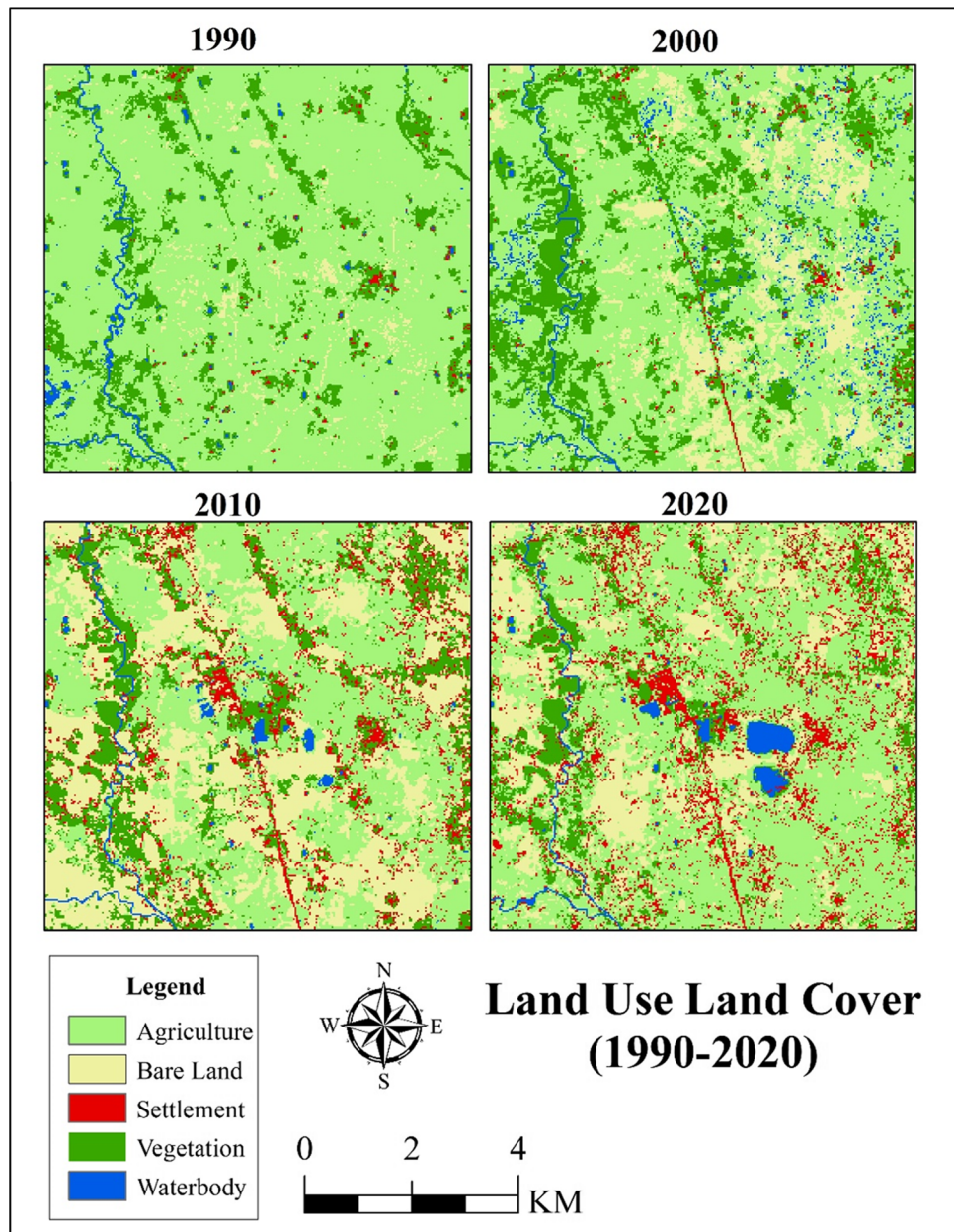
### Transition of Different LULCs

In this study, a transition matrix was employed to analyze the transformation of different landforms. The results, as depicted in Figs. 3 and 4, demonstrate a transition matrix scenario over a period of 30 years, during which a total change of approximately 2564.19 hectares was observed between 1990 and 2020. Approximately 45.71% of agricultural land was converted to bare land, while 14.58% of agricultural land was transformed into vegetation. Conversely, 16% of vegetation was converted to agricultural land and 10.63% of the agricultural area was transformed into settlement areas.

**Table 6** LULC changes data

LULC categories	1990–2000		2000–2010		2010–2020		Overall change 1990–2020	
	Change in area (ha)	(%)	Change in area (ha)	(%)	Change in area (ha)	(%)	Change in area (ha)	(%)
Agriculture land	-1305	-20.53	-1446.93	-22.74	+1317.51	+19.33	-1434.42	-23.94
Bare land	+695.16	+10.94	+1418.4	+22.31	-1070.73	-17.31	+1042.83	+15.94
Vegetation	+436.59	+6.87	-258.3	-4.06	-387	-6.33	-208.71	-3.52
Settlement	+51.3	+0.80	+419.4	+6.60	+250.38	+3.65	+721.08	+11.05
Water bodies	+121.95	+1.92	-132.57	-2.09	+45.18	+0.66	+34.56	+0.49

**Fig. 2** Temporal analysis of LULC pattern of the study area (1990 to 2020)



## LST Change

Impermeable surfaces, such as barren land and settlements, heat up quickly when exposed to sunlight, especially between the hours of 8:00 a.m. and 12:00 p.m. (Bendib et al. 2017). The findings of this study indicate that over the last 30 years, there has been a substantial increase in LST due to a dramatic rise of impervious surfaces in the high-temperature zone (Fig. 5).

Table 7 displays the maximum, minimum, mean, and standard deviation of LST for various years. The maximum temperature jumped from 23.28 °C in 1990 to 29.87 °C in 2020. Moreover, the minimum temperature also changed throughout time, with the lowest temperature (17.97 °C)

recorded in 2010. The table shows that the mean temperature increased from 21.43 to 21.91 °C in the past three decades. The largest deviation detected in 2010 was 1.38, and the lowest in 1990 was 0.59. According to the analysis, mean temperature increased by 0.015 °C/30ya (30ya denotes 30 years) and the maximum temperature increased by 0.219 °C/30ya throughout the 30 years (1990 to 2020).

## LST Zone Classification

LST zone has been classified into four categories for each year such as very low temperature, low temperature, medium temperature, and high temperature zone (Fig. 6). Each zone holds LST distribution over different LULCs.

**Fig. 3** Transition matrix of study area from 1990 to 2020 in a Sankey diagram

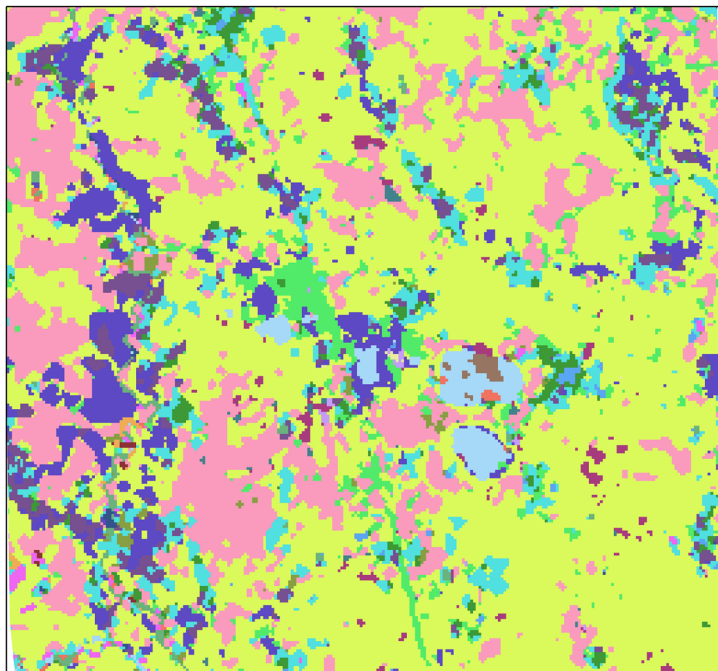
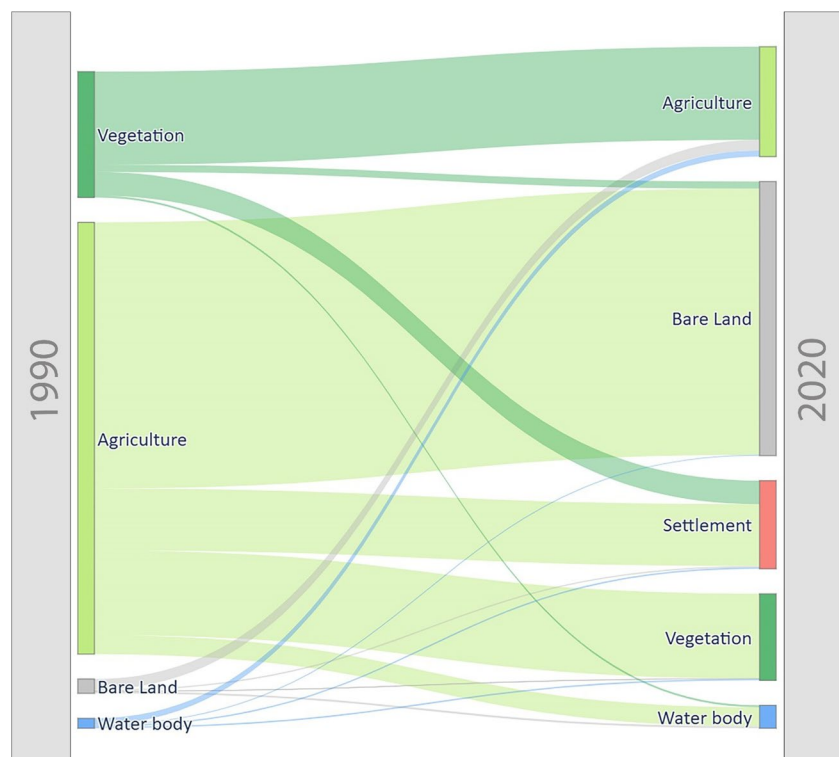


**Fig. 4** Transition of different LULCs from 1990 to 2020

Table 8 shows a chronological LST increase observed over the medium and high zone. It is observable that LST increased drastically in the high zone from 1990 to 2020.

However, Table 9 shows the LULC distribution over different LST zones. As per the findings, the maximum areas of Barapukuria were classified as medium LST zone

**Fig. 5** Changing pattern of LST from 1990 to 2020

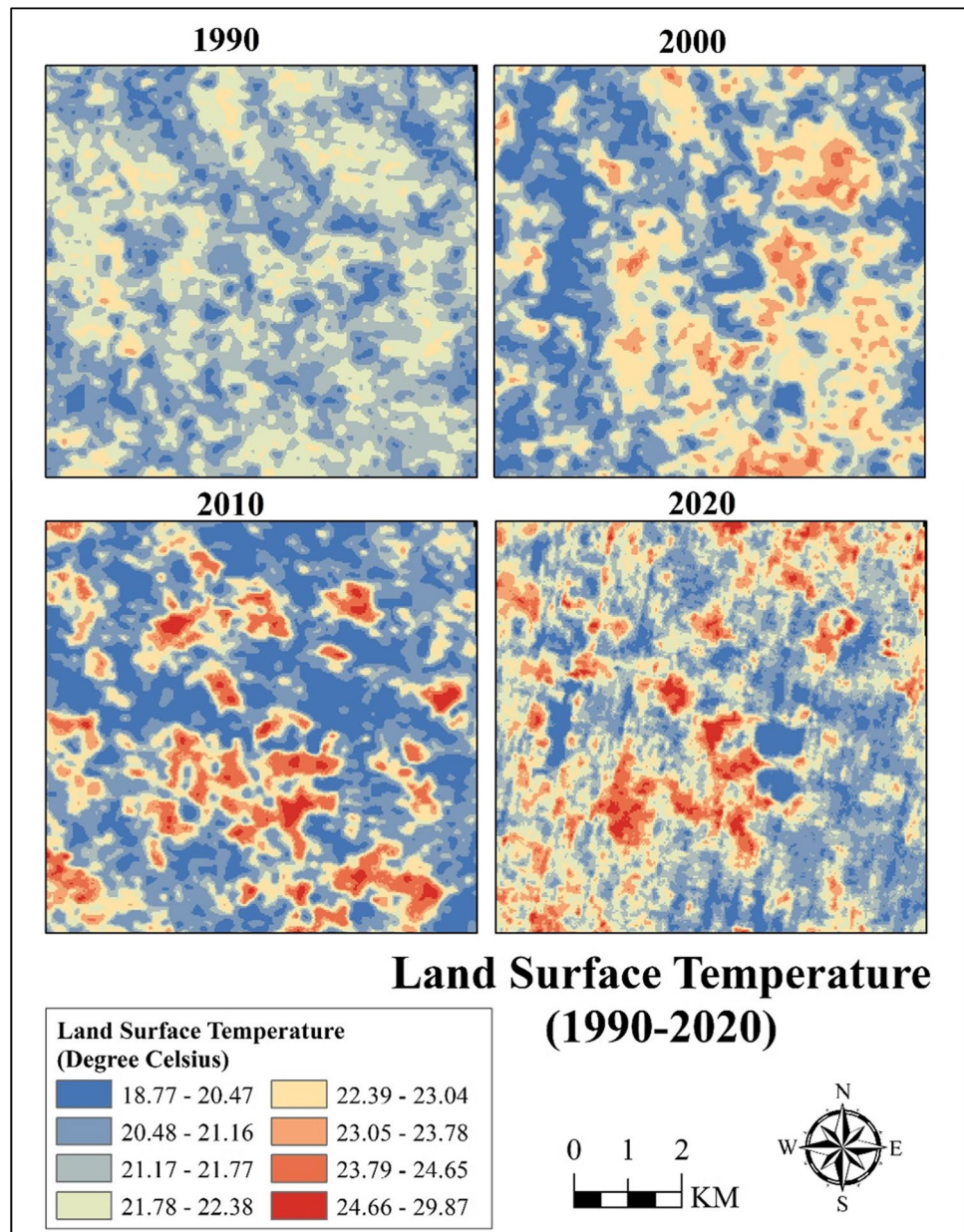


**Table 7** Descriptive statistics of LST

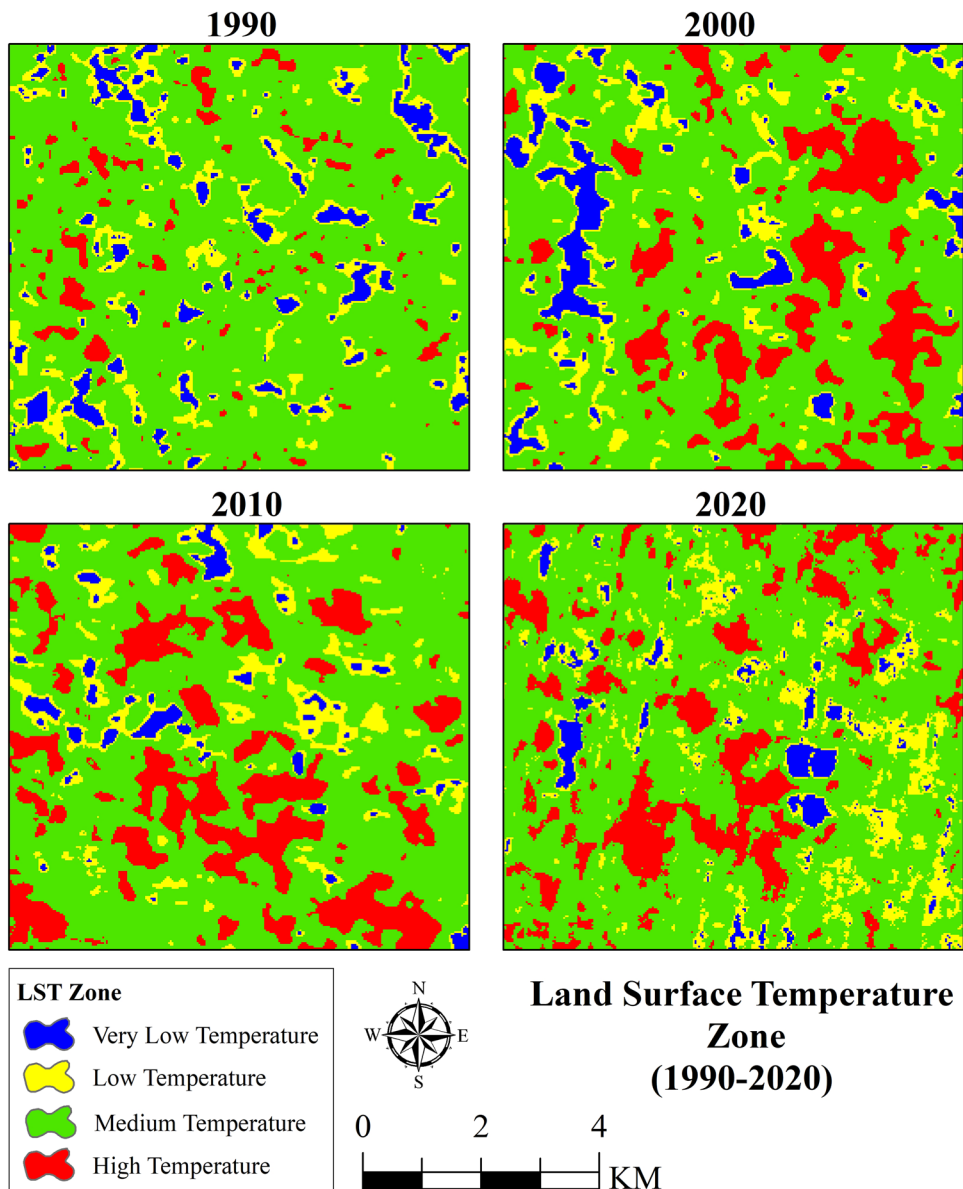
Years	Maximum	Minimum	Mean	Standard deviation
1990	23.28	19.05	21.43	0.59
2000	24.59	18.30	21.51	1.07
2010	26.41	17.97	21.45	1.38
2020	29.87	18.77	21.91	1.13

in every decade where agriculture land was dominant LULC for each decade. On the other hand, bare land has become dominant in the high zone in the last two decades.

### LULC and LST Relation

Figure 7 depicts the relationship between the LULC and the average LST of each year. Over the past three decades, agricultural land and water bodies have not experienced any significant changes in LST, except for a minor decrease in temperature in 2010 for agricultural land and a slight increase in temperature in 2000 for water bodies in Barapukuria. However, the LST of bare land and settlement has drastically increased in the past 30 years.

Furthermore, in 2000, the LST line was increased, because bare land retained more heat than other land cover

**Fig. 6** LST zone (1990–2020)

categories. In 2010, a slight LST drop found on agriculture and waterbodies from previous decade. However, in 2020, there was a significant increase in LST detected for bare land, vegetation, and settlements (Fig. 7).

#### Correlation Between LST and Biophysical Parameters

Figure 8 demonstrates that the NDVI has a moderate negative relation with LST in 1990 and 2000 (Fig. 8a, b). This relation has become very low negative and positive in 2010 and 2020, respectively (Fig. 8c, d). NDBI has strong positive relation with LST from 1990 to 2010 (Fig. 8e–g). On the other hand, DBSI has moderate to strong positive and moderate to negative relations with LST each year (Fig. 8i–l). NDMI has moderate to strong negative relations with LST each year (Fig. 8m–p). As built-up materials and bare surfaces have lower specific heat capacity, it exerts a positive association with LST. After the operation of coal extraction and power plant in the study area, the settlement has been growing day by

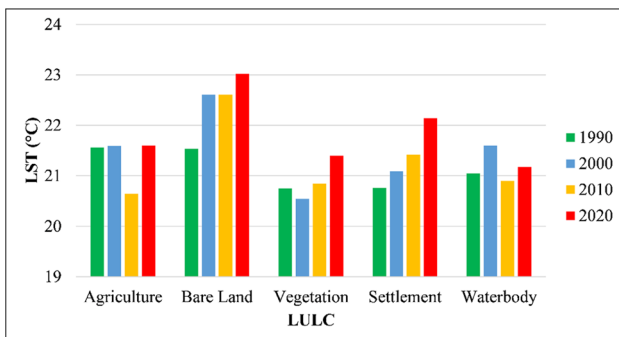
**Table 8** LST distribution (degree Celsius) by zones

Zone	1990	2000	2010	2020
Very low	19.05–20.54	18.3–19.81	17.97–19.3	18.76–20.2
Low	20.54–20.71	19.95–20.21	19.53–20.06	20.21–20.76
Medium	20.88–21.99	20.46–22.5	20.07–22.83	20.77–23.03
High	22.33–23.28	22.76–24.58	22.84–26.4	23.04–29.86

**Table 9** LULC distribution (hectare) by LST zones

LST zone	LULC	1990	2000	2010	2020
Very low	Agriculture	151.83	137.34	163.44	92.88
	Bare land	2.97	1.35	0.63	0.81
	Settlement	198.54	232.74	19.17	62.37
	Vegetation	8.73	5.67	0.81	7.74
	Waterbody	17.37	16.65	14.67	55.26
	<b>Total</b>	<b>379.44</b>	<b>393.75</b>	<b>198.72</b>	<b>219.06</b>
Low	Agriculture	360.54	300.24	462.69	572.76
	Bare land	12.78	7.11	6.48	4.59
	Settlement	322.2	305.73	86.94	85.14
	Vegetation	15.75	12.15	10.71	47.25
	Waterbody	24.66	14.85	10.8	17.64
	<b>Total</b>	<b>735.93</b>	<b>640.08</b>	<b>577.62</b>	<b>727.38</b>
Medium	Agriculture	4357.35	2885.49	1683.45	2639.97
	Bare land	178.47	407.7	1249.2	648.18
	Settlement	336.6	759.15	911.88	475.2
	Vegetation	15.57	70.2	440.82	567.45
	Waterbody	63.9	162.27	61.56	54.45
	<b>Total</b>	<b>4951.89</b>	<b>4284.81</b>	<b>4346.91</b>	<b>4385.25</b>
High	Agriculture	291.06	531.54	92.88	269.73
	Bare land	5.22	478.35	1062.63	588.51
	Settlement	5.49	2.43	23.13	27.72
	Vegetation	0	3.33	58.95	138.42
	Waterbody	2.25	36.99	10.44	15.21
	<b>Total</b>	<b>304.02</b>	<b>1052.64</b>	<b>1248.03</b>	<b>1039.59</b>

The bold entries indicating the total calculated area for different land cover for the year of 1990, 2000, 2010 and 2020

**Fig. 7** LST distribution by LULC

day (Table 6). With local urbanization, enormous legal/illegal brick kilns/industries have been developed in the adjacent area, which is producing heat. Moisture has a higher heat transfer capacity, so it can lower LST fast. Apart from general scenario, NDVI has shown very low relation with LST in 2010 and 2020 (Fig. 8c, d). As bare land is the dominant LULC in the study area in each year (Fig. 7), bare land exhibits low NDVI, so it is causing an anomaly in the correlation between NDVI and LST (Hao et al. 2012; Alademomi et al. 2022).

## Nature of LST Increase for Different LULCs

According to LULC change maps, surface temperatures have risen significantly in areas where settlement and bare land dominate LULC categories. The LST increase rate of bare land is the highest, which is about 0.049 °C/year. The settlement also confronted high temperature increasing rate of about 0.45 °C/Dec. The decadal change of LST for vegetation was about 0.22 °C. Agricultural land showed a little variation in temperature as maximum agricultural fields were filled with paddy with fewer varieties. The agricultural land temperature increased by only 0.034 °C during these 30 years (Table 10).

## Discussion

Changes in LULC can have a substantial effect on LST in areas with coal mines. Deforestation, land use changes, and land degradation are all outcomes of coal mining operations that can alter LST and the surface energy balance. For instance, the loss of vegetation and topsoil during coal mining can raise LST by increasing surface albedo and lowering evapotranspiration. Moreover, bare soil or exposed rocks may increase the land surface's thermal conductivity and heat capacity, causing greater daytime temperatures and lower nighttime temperatures. Moreover, the use of mining equipment, processing facilities, and other industrial processes can generate waste heat that might contribute to the production of LST in the nearby areas. The urban heat island effect, where temperatures are much higher in urbanized areas than in the nearby rural areas, can be brought on by this waste heat. In addition, the changing wind patterns, lower humidity, and higher dust and air pollution in coal mine sites can lead to changes in the microclimate, which can further influence LST.

LULCs have a major effect on LST. The amount of incoming solar radiation that is absorbed or reflected by the ground surface might vary depending on how the land is used and the type of vegetation cover. For instance, compared to urban regions or bare terrain, which absorb more solar radiation and have a larger heat capacity, locations covered by flora, such as woods or grasslands, typically have a lower LST. The evapotranspiration process, which cools the surface by releasing water vapor into the atmosphere, can also be accelerated by vegetation.

The changing LST with LULC can be visualized by comparing two categorized images of LULC and LST. The following section discusses the visual interpretation of LST changing. According to Fig. 9, agricultural land occupies a large portion of the study area, and the maximum area has a low LST. By comparing the LST map with the LULC map, it is observable that agricultural

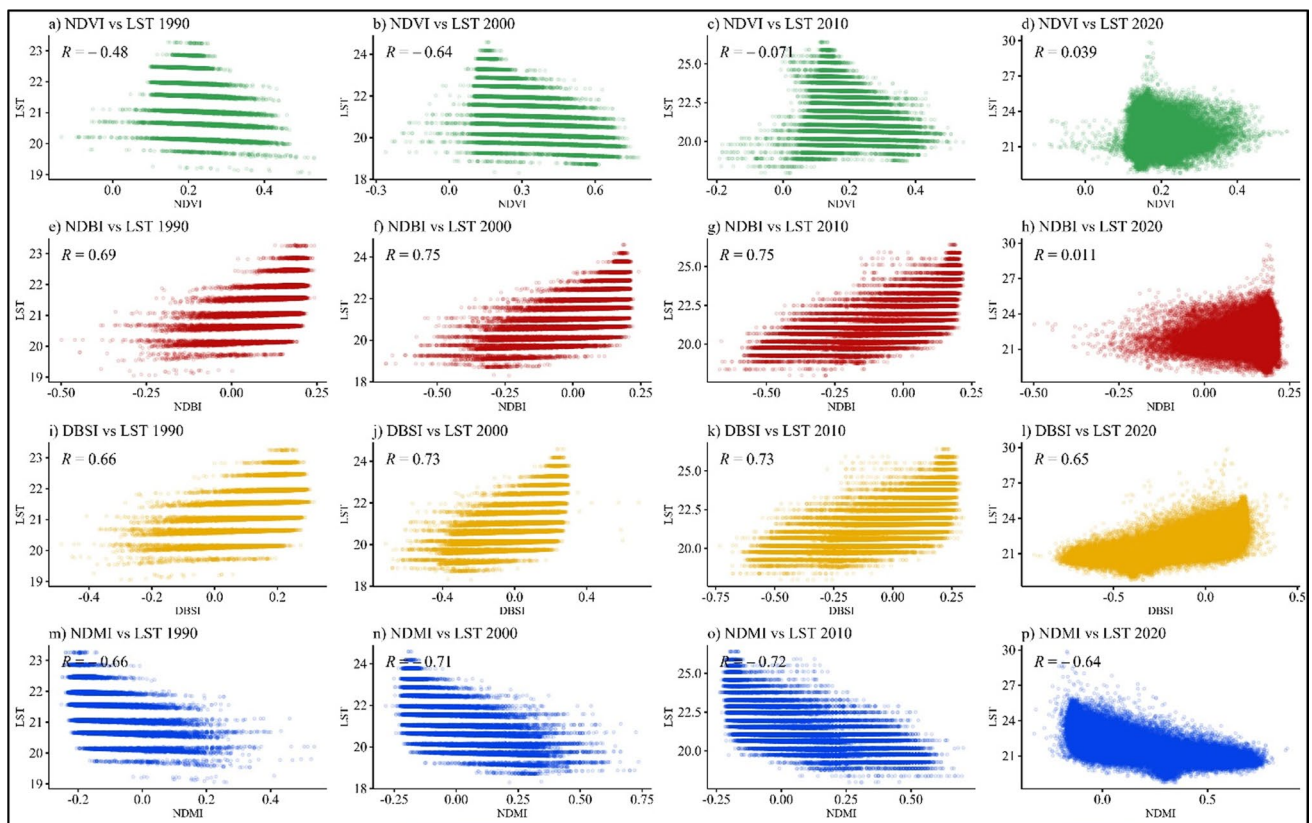


**Fig. 8** Pearson's correlation between LST and biophysical parameters

**Table 10** Nature of LST increase for different LULC categories

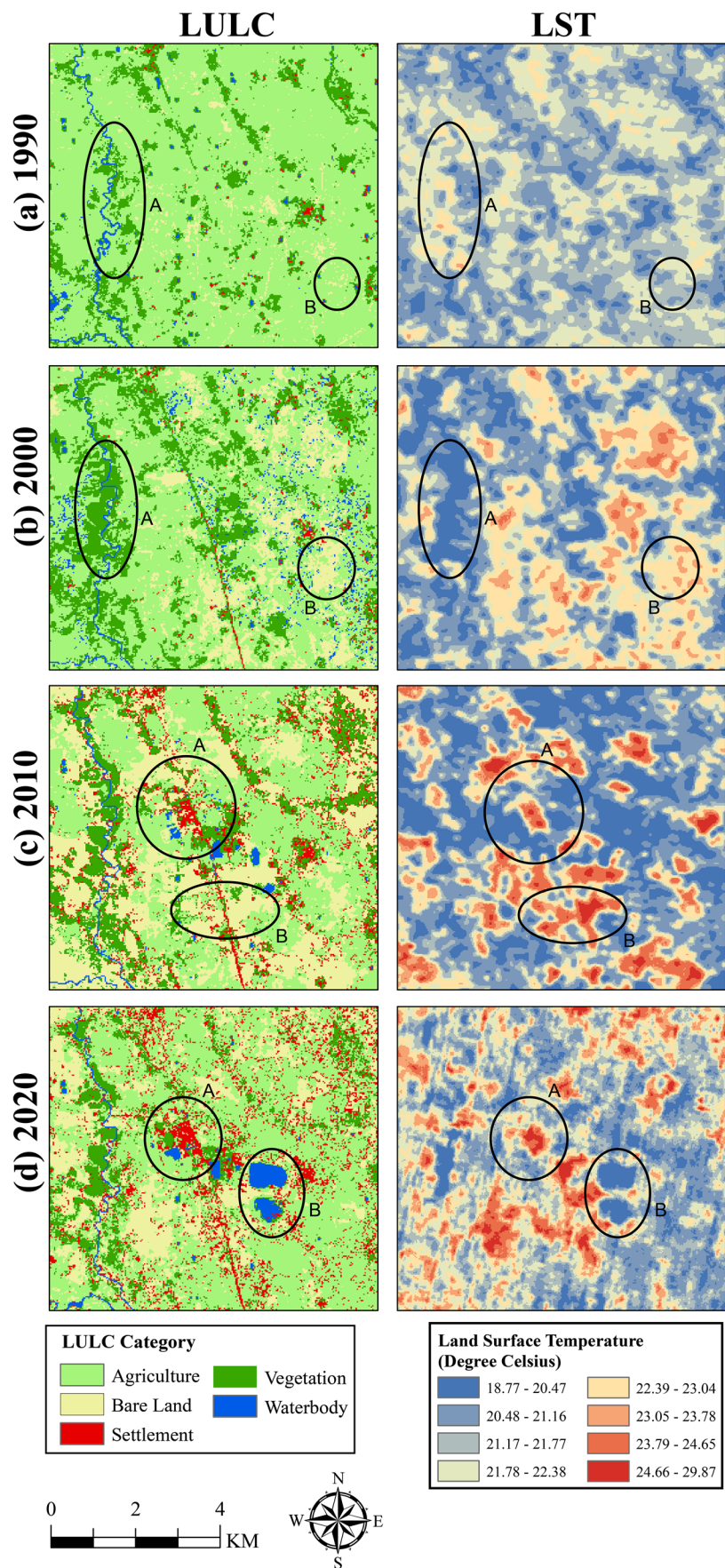
LULC	Increase in °C	Yearly increase	Decadal increase
Agriculture land	0.035	0.001	0.012
Bare land	1.477	0.049	0.492
Vegetation	0.649	0.022	0.216
Settlement	1.373	0.046	0.458
Waterbodies	0.121	0.004	0.040

and vegetative areas have relatively lower LST values for all timescales. In contrast, settlement and bare land has higher LST value which gradually increased over time. The LULC map demonstrates that the areas marked as point A in Fig. 9a, which are surrounded by bodies of water, exhibit notably higher LST. In addition, the LULC is almost all barren terrain on the LULC map, and some of that bare area has a low LST because of vegetation (pointed out as B in Fig. 9b). The differences between the LST from Fig. 9b and the LULC map are easily seen. As shown in Fig. 9b, the vegetation with a water body has the lowest LST, which is less than roughly 20 °C. In 1990, the highest LST was detected in a bare area previously covered by agricultural land and plants.

The LST in the desolate terrain area ranges from 22 to 24 °C. Due to grown-up bare land regions, the LST of the study area has increased since 1990, as seen by the density of the LST map this year. The visual differences between the LULC and LST maps of the year 2010 can be distinguished easily. Figure 9c shows that the bare land area increases considerably, which causes the increase of LST. The temperatures in some bare land areas exceed 26 °C. The settlement area does not show any significant difference as the area is not so dense and covered with vegetation. The vegetation has the lowest LST, less than 20 °C. It should be noted that barren land has a high LST, having been switched from the agricultural and vegetative categories for development purposes. A portion of the bare soil category (indicated as B in Fig. 9c) is transformed from agriculture to a settlement area with time. In 2020, the visual difference can be interpreted significantly (Fig. 9d). The rate of evapotranspiration of the same plant species can vary since it is an essential biological process of the plant and vegetation. As a result, the LST can be varied with different vegetation cover.

The water body has the lowest LST, which is less than 20 °C. However, there is a change in the LULC settlement category this year. The high LST is caused by an increase in bare land, which has led to an expansion in settlement

**Fig. 9** Visual interpretation of LST to LULC transition (1990–2020)



areas. Point B, which displays the disastrous change of LST to the LULC map, stands out as a significant divergence. In this area, the highest LST is above 28 °C. The highest LST point region has a body of water; however, this water is utilized to cool the power plant's reactor, which becomes hot and has the highest LST. Another water reservoir near the coal mine mostly holds underground mining discharge has a lower temperature.

## Conclusion

In conclusion, the study aimed to examine the impact of human activities on LST in the Barapukuria coal mine area. The results showed a decline in agricultural land by 23.94% and an increase in bare land and settlement areas by 15.94% and 11.05% respectively in the last 30 years. The LST analysis indicated an upward trend for all LULC categories, with highest value for bare land (1.477 °C) and settlement (1.373 °C) and the lowest value for vegetation (0.649 °C), water-bodies (0.121 °C), and agricultural land (0.035 °C) in the past three decades. The correlation analysis between LST and biophysical parameters revealed that the increase in LST was related to settlement and bare land. The visual interpretation analysis demonstrated that LST is dependent on the changing LULC with an increase in settlement and bare soil land categories leading to an increase in LST values.

Consequently, the decline in agricultural land and substantial rise of bare land and settlement areas have significant impact on the surrounding environment and the overall well-being of the community. Against the background of global climate change, the rising LST particularly poses a threat to the ecosystem and human health. A comprehensive and sustainable approach to land use plan and management is required. This approach should consider the interplay between human activities, environmental conservation, and community well-being, considering not only the size and distribution of different landforms but also other biophysical parameters such as vegetation cover, soil moisture, and surface albedo. With the rapid industrialization and urbanization in recent decades, LULC has undergone dramatic changes in many nations of the global south. The issue of rising LST is a common occurrence among many nations in the region, so it is advised that policymakers in these nations adopt certain strategies to encourage sustainable development and enhance living conditions. Specifically, during urban development, thoughtful and sustainable land use plans need to be designed and implemented. Sufficient greenspace such as recreational parks and gardens need to be constructed alongside residential and industrial zones to mitigate urban heat island effects. The wasteland and arid landscapes need to be reforested and revegetated through conscious conservation efforts. To ensure the effectiveness of

these efforts, the local communities that are deeply affected by the dramatic LULC changes need to be engaged. First, education campaigns need to be organized to raise public awareness of the connection between LULC and rising LST. Schools and community events are often the best starting places. Second, stakeholders from diverse sociodemographic backgrounds need to be actively involved in the comprehensive land use planning process. Their input reflecting their needs for their well-being need to be incorporated into the plan. In doing so, potential tensions and conflicts between the government and local community can be eased and reduced. Third, grass-root environmental organizations often play a crucial role in raising awareness of environmental issues and mobilizing community members to adopt environmentally sustainable actions. As a result, funding agencies, either governmental or non-governmental, should provide support and resources to these organizations who can facilitate actions. These actions are believed to effectively control the rising temperatures and promote a healthy and sustainable environment for the community of global south. The results of this study can offer Bangladesh and other developing nations in the global south evidence-based recommendations for sustainable development.

**Data Availability** Data will be available based on reasonable request.

## Declarations

**Ethical Approval** This manuscript represents core research and has not yet been published or submitted anywhere. All the data sources were cited properly. The authors have obtained all the ethical approvals about this paper. The authors declare to obey all the academic ethical standards.

**Informed Consent** All the authors who made contributions to this paper are included and aware of the content of this paper. They also agree to submit this paper to the Journal of Geovisualization and Spatial Analysis.

**Conflict of Interest** The authors declare no competing interests.

## References

- Adiguzel F, Cetin M, Dogan M, Gungor S, Kose M, Bozdogan Sert E, Kaya E (2022) The assessment of the thermal behavior of an urban park surface in a dense urban area for planning decisions. *Environ Monit Assess* 194(7):519
- Ahmed B (2011) Urban land cover change detection analysis and modeling spatio-temporal growth dynamics using remote sensing and GIS techniques: a case study of Dhaka, Bangladesh (Doctoral dissertation). The Universidade Nova de Lisboa
- Ahmed Z, Alam R, Hussain AB, Ambinakudige S, Chowdhury TA, Kabir MN et al (2022) Agricultural land conversion and land surface temperature change in four industrial areas in Bangladesh: results from remote sensing and DPSIR approach. *Arab J Geosci* 15(10):932

- Alademomi AS, Okolie CJ, Daramola OE, Akinnusi SA, Adediran E, Olanrewaju HO et al (2022) The interrelationship between LST, NDVI, NDBI, and land cover change in a section of Lagos metropolis, Nigeria. *Appl Geomat* 14(2):299–314
- Amare MT, Demissie ST, Beza SA, Erena SH (2023) Land cover change detection and prediction in the Fafan catchment of Ethiopia. *J Geovis Spat Anal* 7(2):19
- Artis DA, Carnahan WH (1982) Survey of emissivity variability in thermography of urban areas. *Remote Sens Environ* 12(4):313–329
- Bagwan WA, Sopan Gavali R (2023) Dam-triggered land use/land cover change detection and comparison (transition matrix method) of Urmadi river watershed of Maharashtra, India: a remote sensing and GIS approach. *Geol Ecol Landsc* 7(3):189–197
- Bajocco S, De Angelis A, Perini L, Ferrara A, Salvati L (2012) The impact of land use/land cover changes on land degradation dynamics: a Mediterranean case study. *Environ Manag* 49:980–989
- Balogun I, Ishola K (2017) Projection of future changes in landuse/landcover using cellular automata/Markov model over Akure City, Nigeria. *J Remote Sens Technol* 5(1):22–31
- Bappa SA, Malaker T, Mia MR, Islam MD (2022) Spatio-temporal variation of land use and land cover changes and their impact on land surface temperature: a case of Kutupalong Refugee Camp, Bangladesh. *Heliyon* 8(9):e10449
- Barry RG, Chorley RJ (2009) Atmosphere, weather and climate. Routledge
- Bendib A, Dridi H, Kalla MI (2017) Contribution of Landsat 8 data for the estimation of land surface temperature in Batna city, Eastern Algeria. *Geocarto Int* 32(5):503–513
- Bonafoni S, Anniballe R, Gioli B, Toscano P (2016) Downscaling Landsat land surface temperature over the urban area of Florence. *Eur J Remote Sens* 49(1):553–569
- Cao JS, Deng ZY, Li W, Hu YD (2020) Remote sensing inversion and spatial variation of land surface temperature over mining areas of Jixi, Heilongjiang, China. *PeerJ* 8:e10257
- Carlson TN, Ripley DA (1997) On the relation between NDVI, fractional vegetation cover, and leaf area index. *Remote Sens Environ* 62(3):241–252
- Cetin M, Adiguzel F, Kaya O, Sahap A (2018) Mapping of bioclimatic comfort for potential planning using GIS in Aydin. *Environ Dev Sustain* 20:361–375
- Chaddad F, Mello FA, Tayebi M, Safanelli JL, Campos LR, Amorim MTA et al (2022) Impact of mining-induced deforestation on soil surface temperature and carbon stocks: a case study using remote sensing in the Amazon rainforest. *J South Am Earth Sci* 119:103983
- Choudhury D, Das K, Das A (2019) Assessment of land use/land cover changes and its impact on variations of land surface temperature in Asansol-Durgapur Development Region. *Egypt J Remote Sens Space Sci* 22(2):203–218
- Chowdhury TA, Islam MS (2022) Assessing and simulating impacts of land use/land cover changes on land surface temperature in Mymensingh City, Bangladesh: 10.32526/ennrj/20/202100110. *Environ Nat Resour J* 20(2):110–128
- Chughtai AH, Abbasi H, Karas IR (2021) A review on change detection method and accuracy assessment for land use/land cover. *Remote Sens Appl: Soc Environ* 22:100482
- Cui J, Zhu M, Liang Y, Qin G, Li J, Liu Y (2022) Land use/land cover change and their driving factors in the Yellow River Basin of Shandong Province based on Google Earth Engine from 2000 to 2020. *ISPRS Int J Geo-Inform* 11(3):163
- Derome J, Lukina N (2010) Interaction between environmental pollution and land-cover/land-use change in Arctic areas. In: Eurasian Arctic land cover and land use in a changing climate. Springer Netherlands, Dordrecht, pp 269–289
- Fu P, Weng Q (2018) Responses of urban heat island in Atlanta to different land-use scenarios. *Theor Appl Climatol* 133(1):123–135
- Hao F, Zhang X, Ouyang W, Skidmore AK, Toxopeus AG (2012) Vegetation NDVI linked to temperature and precipitation in the upper catchments of Yellow River. *Environ Model Assess* 17:389–398
- Hasan MA, Mia MB, Khan MR, Alam MJ, Chowdury T, Al Amin M, Ahmed KMU (2023) Temporal changes in land cover, land surface temperature, soil moisture, and evapotranspiration using remote sensing techniques—a case study of Kutupalong Rohingya Refugee Camp in Bangladesh. *J Geovis Spat Anal* 7(1):11
- Hathout S (2002) The use of GIS for monitoring and predicting urban growth in East and West St Paul, Winnipeg, Manitoba, Canada. *J Environ Manag* 66(3):229–238
- Hossain M, Paul SK, Hasan M (2015) Environmental impacts of coal mine and thermal power plant to the surroundings of Barapukuria, Dinajpur, Bangladesh. *Environ Monit Assess* 187(4):1–11
- Hu Y, Jia G, Pohl C, Zhang X, van Genderen J (2016) Assessing surface albedo change and its induced radiation budget under rapid urbanization with Landsat and GLASS data. *Theor Appl Climatol* 123:711–722
- Hussain M, Alak P, Azmz I (2016) Spatio-temporal analysis of land use/land cover changes in Chittagong city corporation, Bangladesh. *Int. J. Adv. Remote Sens. GIS Geogr* 4:56–72
- Jensen JR (1996) Introductory digital image processing: a remote sensing perspective (No. Ed. 2). Prentice-Hall Inc
- Kachhwala TS (1985) Temporal monitoring of forest land for change detection and forest cover mapping through satellite remote sensing. In: Proceedings of the 6th Asian Conf. on Remote Sensing, Hyderabad, 1985 (pp. 77–83)
- Koko AF, Yue W, Abubakar GA, Alabsi AAN, Hamed R (2021) Spatiotemporal influence of land use/land cover change dynamics on surface urban heat island: a case study of Abuja metropolis, Nigeria. *ISPRS Int J Geo-Inform* 10(5):272
- Koppen W (1936) Das geographische System der Klimate. Handbuch der Klimatologie
- Landsat, N. A. S. A. (2011) Science data users handbook. Retrieved from <https://www.usgs.gov/media/files/landsat-7-data-users-handbook>. Accessed 17 Jan 2021
- Lilly Rose A, Devadas MD (2009) Analysis of land surface temperature and land use/land cover types using remote sensing imagery—a case in Chennai city, India. In: The seventh international conference on urban clim held on (Vol. 29)
- Liu C, Li W, Zhu G, Zhou H, Yan H, Xue P (2020) Land use/land cover changes and their driving factors in the Northeastern Tibetan Plateau based on Geographical Detectors and Google Earth Engine: a case study in Gannan Prefecture. *Remote Sens* 12(19):3139
- Mahi MM, Sharif MS, Rudra RR, Haque MN (2021) The geo-spatial approach to detect the change in vegetation and land surface temperature (LST) after formation of Rohingya settlements in Bangladesh. *J Civil Eng Sci Technol* 12(2):288–241
- Morshed SR, Fattah MA, Hoque MM, Islam MR, Sultana F, Fatema K et al (2023) Simulating future intra-urban land use patterns of a developing city: a case study of Jashore, Bangladesh. *GeoJournal* 88(1):425–448
- Niyogi D (2019) Land surface processes. In: In Current trends in the representation of physical processes in weather and climate models (pp. 349–370). Springer, Singapore
- Ozesmi SL, Bauer ME (2002) Satellite remote sensing of wetlands. *Wetlands Ecol Manag* 10(5):381–402
- Panah SK, Mogaddam MK, Firoozjai MK (2017) Monitoring spatiotemporal changes of heat island in Babol city due to land use changes. *Int Arch Photogrammetry Remote Sens Spat Inform Sci* 42:17–22
- Rajasekar U, Weng Q (2009) Application of association rule mining for exploring the relationship between urban land surface temperature and biophysical/social parameters. *Photogramm Eng Remote Sens* 75(4):385–396

- Ranagalage M, Murayama Y, Dissanayake DMSLB, Simwanda M (2019) The impacts of landscape changes on annual mean land surface temperature in the tropical mountain city of Sri Lanka: a case study of Nuwara Eliya (1996–2017). *Sustainability* 11(19):5517
- Rashid KJ, Hoque M, Esha TA, Rahman M, Paul A (2021) Spatiotemporal changes of vegetation and land surface temperature in the refugee camps and its surrounding areas of Bangladesh after the Rohingya influx from Myanmar. *Environ Dev Sustain* 23(3):3562–3577
- Rasul A, Balzter H, Ibrahim GRF, Hameed HM, Wheeler J, Adamu B et al (2018) Applying built-up and bare-soil indices from Landsat 8 to cities in dry climates. *Land* 7(3):81
- Rouse Jr, John W, Hect Haas R, Deering DW, Schell JA, Harlan JC (1974) Monitoring the vernal advancement and retrogradation (green wave effect) of natural vegetation (No. E75-10354)
- Roxburgh T, Ellis K, Johnson J, Baldos UL, Hertel T, Nootenboom C, Polasky S (2020) Global future: assessing the global economic impacts of environmental change to support policymaking
- Roy PS, Ramachandran RM, Paul O, Thakur PK, Ravan S, Behera MD et al (2022) Anthropogenic land use and land cover changes—a review on its environmental consequences and climate change. *J Indian Soc Remote Sens* 50(8):1615–1640
- Saini V, Gupta RP, Arora M K (2016) Environmental impact studies in coalfields in India: a case study from Jharia coal-field. *Renew Sustain Energy Rev* 53:1222–1239
- Skole D, Tucker C (1993) Tropical deforestation and habitat fragmentation in the Amazon: satellite data from 1978 to 1988. *Science* 260(5116):1905–1910
- Sobrino JA, Jiménez-Muñoz JC, Paolini L (2004) Land surface temperature retrieval from Landsat TM 5. *Remote Sens Environ* 90(4):434–440
- Thapa RB, Murayama Y (2009) Examining spatiotemporal urbanization patterns in Kathmandu Valley, Nepal: remote sensing and spatial metrics approaches. *Remote Sens* 1(3):534–556
- Trolle D, Nielsen A, Andersen HE, Thodsen H, Olesen JE, Børgeesen CD et al (2019) Effects of changes in land use and climate on aquatic ecosystems: coupling of models and decomposition of uncertainties. *Sci Total Environ* 657:627–633
- Wang SW, Gebru BM, Lamchin M, Kayastha RB, Lee WK (2020) Land use and land cover change detection and prediction in the Kathmandu district of Nepal using remote sensing and GIS. *Sustainability* 12(9):3925
- Weng Q, Lu D, Schubring J (2004) Estimation of land surface temperature–vegetation abundance relationship for urban heat island studies. *Remote Sens Environ* 89(4):467–483
- Wilson EH, Sader SA (2002) Detection of forest harvest type using multiple dates of Landsat TM imagery. *Remote Sens Environ* 80(3):385–396
- Zha Y, Gao J, Ni S (2003) Use of normalized difference built-up index in automatically mapping urban areas from TM imagery. *Int J Remote Sens* 24(3):583–594

**Publisher's Note** Springer Nature remains neutral with regard to jurisdictional claims in published maps and institutional affiliations.

Springer Nature or its licensor (e.g. a society or other partner) holds exclusive rights to this article under a publishing agreement with the author(s) or other rightsholder(s); author self-archiving of the accepted manuscript version of this article is solely governed by the terms of such publishing agreement and applicable law.